Étude du comportement dynamique d'un ressort et d'une rondelle Belleville en Alliage à Mémoire de Forme et évaluation de leur pouvoir amortissant.

Frédéric Thiebaud, Tarak Ben Zineb

Experimental and finite element analysis of superelastic behaviour of Shape Memory Alloy for damping applications

F. THIEBAUD[a,b], T. BEN ZINEB[a,b,c]

a. *Université de Lorraine, LEMTA UMR7563, 54500 Vandoeuvre les Nancy, France*
b. CNRS, LEMTA UMR 7563, 54500 Vandoeuvre les Nancy, France
c. Department of Mechanical Engineering, Khalifa University, PO Box 127788, Abu Dhabi, UAE

Abstract :

Shape memory alloys (SMA) are good candidates especially for being used as passive dampers. In order to develop the use of these alloys in structural vibrations control, the dynamical behavior of a NiTi helical spring is leaded, and the damping effect investigated. First, compression tests on the spring are carried out. These tests allow us to notice the effect of the maximal compression displacement, the cyclic behavior and the compression rate on its mechanical behavior. A finite element model analysis of the compression tests is then proposed. In consequence the materials parameters have been identified after a numerical convergence test. In order to characterize the dynamical behavior of the spring, the innovative tool called equivalent complex stiffness is developed and used. Finally, the one degree of freedom vibration equation is solved with this equivalent complex stiffness. The solution of this equation clearly shows the non linear dynamical behavior of the SMA spring and its damping potential.

Mots clefs : Shape Memory Alloy, experimental compression test, phenomenological model, finite element analysis, equivalent complex stiffness, dynamical behavior.

1 Introduction

Shape memory alloys (SMA) are widely studied as smart materials because of their potentiality to be used as dampers, absorbers or actuators elements. For damping applications, an understanding of the material dynamic behavior is needed. One uses the loss of stiffness linked to the martensite transformation between the mother phase called austenite (A) and the product phase called martensite (M). In this case, the SMA elements are used as absorbers mainly for seismic applications [1-5]. In the present paper, the damping effect of a superelastic NiTi helical spring in compression is investigated. One notices that the study of such a device has been studied in previous investigations, experimentally by Speicher et al. [6], numerically by Mirzaeifar [7]. Nevertheless, a lack of results on the damping effect is still present. Thus, an innovative model of the damping effect is proposed in this paper. To do this, in a first step, experimental compression test are leaded. In a second step, a three dimensional (3D) model implemented in ABAQUS© is used to simulate the compression cycles. A comparison between the experimental and the numerical investigations is done in order to validate the 3D model implementation. In the third part, the equivalent complex stiffness is described and the damping evolutions are investigated. Finally, the dynamic behavior of the helical spring is quickly carried out with the Bode diagrams.

2 Experimental investigations

2.1 Experimental protocol

By considering the geometrical parameters of the SMA helical spring on the figure 1(a), a specific compression tool designed for the spring was adapted on a 100 kN Zwick-Roell© tensile test machine shown on the figure 1(b).

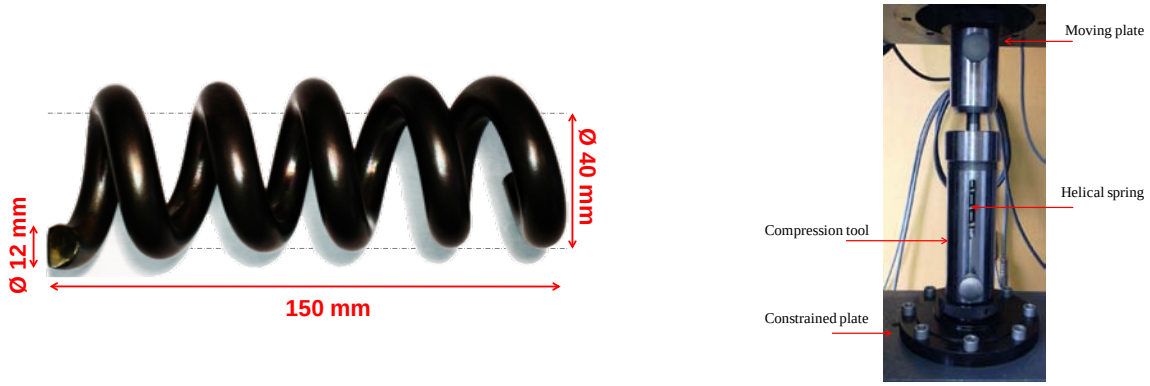

(a) (b)

FIG. 1 – Design of the helical spring (a) and experimental compression tool (b).

This specific tool allows the test machine to be used in tensile configuration with maximum of safety for the operator. The tests performed are as following: monotonic compression protocol with various maximum deformation, influence of the number of compression cycles and influence of the loading rate.

2.2 Compression tests

The evolution of the resulting compression force versus the displacement of the moving plate is given on the figure 2. A quasi-static loading rate for the testing was set at 2.5 mm/s to eliminate dynamic (thermomechanical coupling) effects. Additionally, all experiments were carried out under ambient temperature in the range of 21-23 °C.

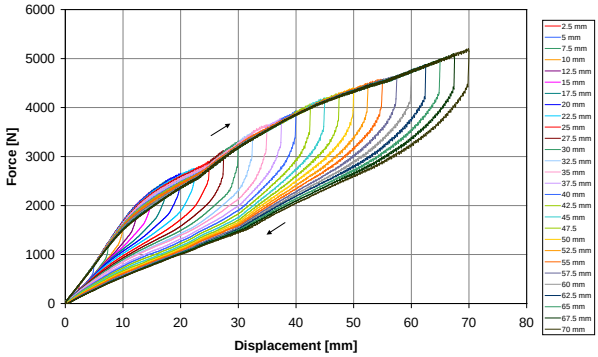

FIG. 2 –Resulting force versus the displacement of the moving plate for different displacement levels.

The typical non linear behavior with hysteresis mechanical of SMA is shown on theses curves. This non linear behavior with hysteresis is explained by the transformation phase (A ↔ M) which operates where the local stress is upper than the beginning forward (reverse) transformation stress. Consequently, this device appears to be a good passive damper.

2.3 Influence of the number of cycles and the loading rate

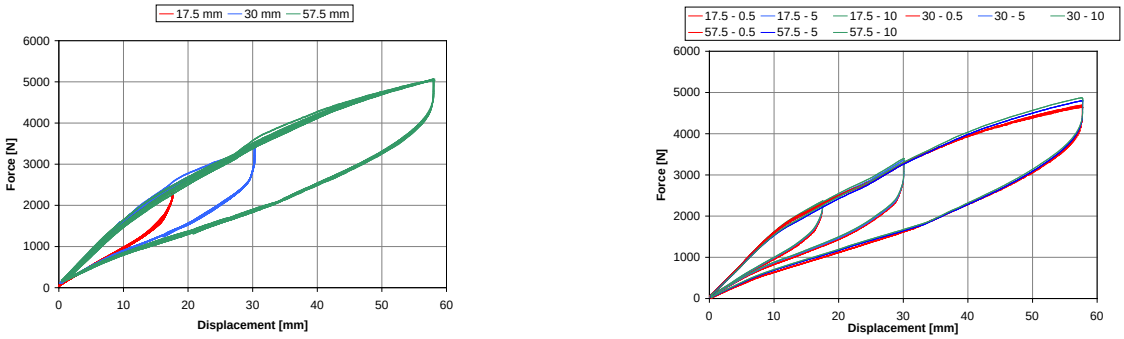

(a) (b)

FIG. 3 – Influence of the number of cycles (a) and the loading rate (b).

30 cycles for three different maximum displacements (17.5 ; 30 and 57.5 mm) are shown on the figure 3(a). Theses curves clearly show that the number of cycles does not affect the mechanical behavior of the helical spring. Furthermore, three different loading rates (0.5 ; 5 and 10 mm/s, $f \approx 0.3\,Hz$) for the same three maximum displacements are tested. Theses curves highlight that the loading rate has no influence on the mechanical behavior too. It is known that the forward transformation (A→M) is exothermal and the reverse transformation (M→A) endothermal. For high loading rates, the helical spring is nevertheless able to quickly evacuate the heat due to the transformation phase.

3 Numerical investigations

3.1 A thermomechanical model for the superelasticity

3.1.1 Statement of thermomechanical dynamical problem

Under the assumptions of small strain and displacements, the thermomechanical problem satisfies the following fundamental equations:

- The mechanical equilibrium :

$$\rho\ddot{\vec{u}} - \vec{\nabla}\cdot\underline{\sigma} = \vec{f} \tag{1}$$

Where ρ represents the material density and $\underline{\sigma}$ the Cauchy stress tensor.

- The first thermodynamic principle (energy conservation without source term) :

$$\rho\dot{e} - \vec{\nabla}\cdot\vec{q} = \underline{\sigma} : \dot{\underline{\varepsilon}} + r \tag{2}$$

Where *e* is the total energy, $\vec{q}$ the vector of thermal flux and $\underline{\varepsilon}$ the Green-Lagrange strain sensor.

- The second thermodynamic principle:

$$\rho T\dot{s} - \rho\cdot r + \vec{\nabla}\cdot\vec{q} - \frac{1}{T}\vec{q}\cdot\vec{\nabla}T \geq 0 \tag{3}$$

Where *s* represents the specific entropy of the material.

3.1.2 Shape memory alloy behavior

The behavior considered in this paper is related to the phase change of SMA. At stress-free state, the material is supposed to be fully austenitic. During the load, the phase can change locally to martensite. The model presented in this paper is motivated by the work of Peultier et al. [8] and improved by Chemisky [9] and Duval [10]. The expression of the Gibbs free energy is defined to describe the two key features described above, which are the introduction of path-dependent transformation strain and the description of the twin accommodation mechanisms.

Two internal variables are used as well: the volume fraction of martensite *f* and the average mean strain $\overline{\varepsilon}_{ij}^{T}$ which can be defined by the following equations :

$$f = V_M / V \text{ et } \overline{\varepsilon}_{ij}^{T} = \frac{1}{V_M}\int_{V_M} \varepsilon_{ij}^{T}(r)dV \tag{4), (5}$$

The transformation strain E_{ij}^{T} can be expressed as follow:

$$E_{ij}^{T} = f\,\overline{\varepsilon}_{ij}^{T} \tag{6}$$

Considering an additive decomposition of strain, the total macroscopic strain E_{ij} is written :

$$E_{ij} = E_{ij}^{el} + E_{ij}^{th} + E_{ij}^{T} \tag{7}$$

Where $\underline{E}^{el}$ et $\underline{E}^{th}$ are respectively the elastic and thermal strain tensor. The derivation of the phenomenological constitutive models for SMA begins with the choice of a thermodynamic free energy potential. As it is developed in Chemisky [8], the following Gibbs free energy potential variation is defined :

$$\Delta G = -\Delta T S^{A} + B\left(T - T_0\right) f - \frac{1}{2}\Sigma_{ij}S_{ijkl}\Sigma_{kl} - f\,\Sigma_{ij}\overline{\varepsilon}_{ij}^{T} - \Sigma_{ij}\alpha\delta_{ij}\left(T - T_{ref}\right) + \frac{1}{2}H_f f^2 + \frac{1}{2}H_\varepsilon f^2 \overline{\varepsilon}_{ij}^{T}\overline{\varepsilon}_{ij}^{T} \tag{8}$$

Where S^A is the entropy of the austenite phase, $B=-\Delta S$ is the difference between the entropy of the austenite and the martensite phases, T is the temperature, H_f and H_ε are interactions parameters, Σ is the macroscopic stress tensor, S is the elastic tensor and α is the thermal expansion coefficient. Thus, driving force variables linked to the internal variables are defined by :

$$F_{\Sigma_{ij}} = -\frac{\partial \Delta G}{\partial \Sigma_{ij}} = S_{ijkl}\Sigma_{kl} + \alpha\delta_{ij}\left(T - T_{ref}\right) + f\,\overline{\varepsilon}_{ij}^{T}\ ,\ F_{\overline{\varepsilon}_{ij}^{T}} = -\frac{\partial \Delta G}{\partial \overline{\varepsilon}_{ij}^{T}} = f\left(\Sigma_{ij}^{dev} - H_\varepsilon \overline{\varepsilon}_{ij}^{T} - \lambda_{ij}^{e}\right) \quad (9)\ (10)$$

$$F_f = -\frac{\partial \Delta G}{\partial f} = -B\left(T - T_0\right) + \Sigma_{ij}\overline{\varepsilon}_{ij}^{T} - \frac{1}{2}H_\varepsilon \overline{\varepsilon}_{ij}^{T}\overline{\varepsilon}_{ij}^{T} - H_f f - \lambda_0 - \lambda_1 \quad (11)$$

Where Σ_{ij}^{dev} is the deviatoric part of the stress tensor. The coefficients λ_0, λ_1 et $\lambda_{ij}^{\varepsilon}$ are Lagrange multipliers due to the physical limitations. They are defined by the following equations :

$$\lambda_0(f) = a_0\frac{f-1}{f},\ \lambda_1(f) = a_1\frac{f}{1-f} \text{ et } \lambda_{ij}^{\varepsilon} = \text{function of } \overline{\varepsilon}_{ij}^{T}, \overline{\varepsilon}_{eq}^{T}, \overline{\varepsilon}^{Sat} \quad (12)$$

3.2 Finite element model description and numerical implementation

The composition of the SMA used in the numerical application is NiTi. Its characteristic phase transformation temperatures measured by electrical resistance evolution are : M_F^0 = 191 K, M_S^0 = 213 K, A_S^0 = 205 K and A_F^0 = 221 K, according to the provider. The material parameters are identified by fitting the experimental curves given in the figure 2 and previous tensile test of the material given in [6], considering a numerical convergence test. The stress distribution is considered converged by using 49731 degrees of freedom.

An appropriate user subroutine (UMAT) is written by C language in the commercially available finite element program ABAQUS©. The spring is modeled three dimensionally with three dimensional quadratic brick elements with reduced integration C3D8R (figure 4(a)). Two rigid surfaces in contact with the spring ends are considered. The lower rigid surface is constrained in all directions and a time varying displacement boundary condition is defined for the upper surface for modeling compression. The supporting shaft in the experiments is modeled with a cylindrical rigid surface inside the helical spring. The automatic time increment option in ABAQUS© is used with an initial guess of dividing the loading and unloading steps into 1000 increments and the non-linear geometry option is activated.

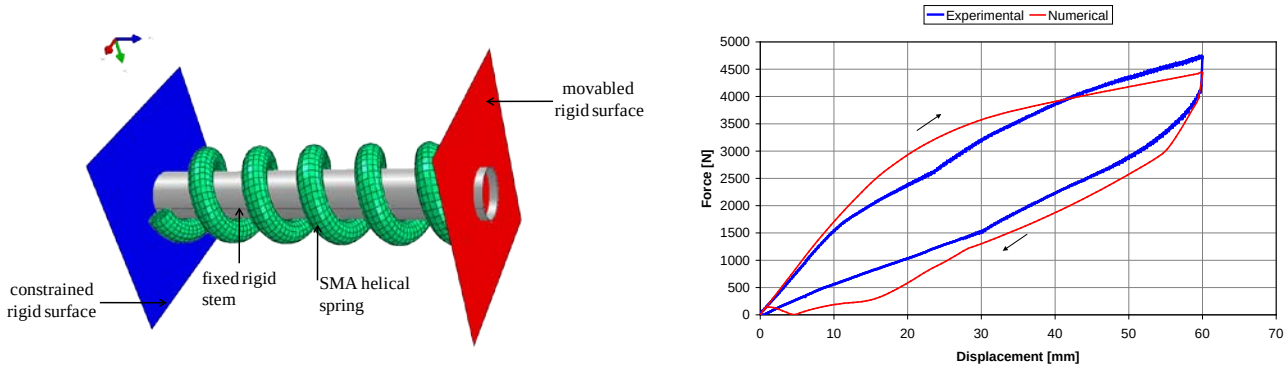

(a) (b)

FIG. 4 – Finite element model of the SMA spring in the initial configuration (a) and comparison between the numerical and the experimental investigations.

3.3 Numerical Results

The load-displacement response for both numerical and experimental cycles is given on the figure 4(b). This first numerical result shows a good correlation between the experimental and the numerical results. It validates the identification of the material parameters and the implementation of the 3D model. The displacement magnitude, the von Mises stress and the volume fraction of martensite are respectively shown

on the figure 5 (a,b,c), for a displacement of the movable plate about 60 mm. One can notice that the transformation phase occurs at this compression level, but no area is totally transformed ($f_{max} = 0.64$). Nevertheless, this is sufficient to confer to the spring the typical non linear hysteresic behavior, oberserved in the experimental part. Now, it is possible to simulate many cycles with different compression ratio, in order to investigate the dynamical behavior of the spring and its damping effect.

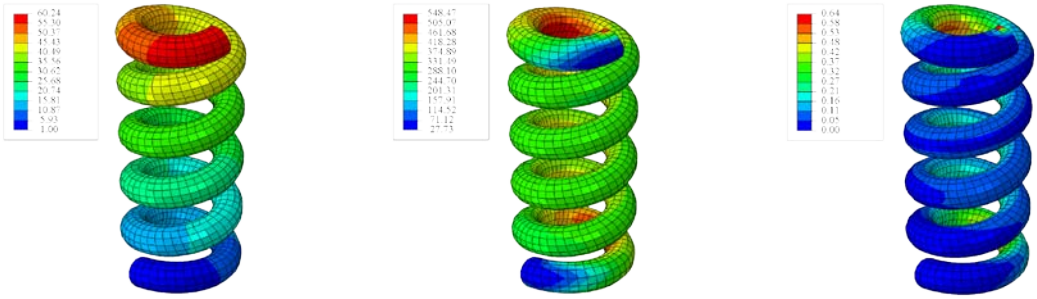

(a) Displacement magnitude [mm] (b) von Mises stress [MPa] (c) Volume fraction of martensite

FIG. 5 – Numerical results at the end of the loading phase (compression displacement about 60 mm).

4 Dynamical behavior and damping effect

4.1 Equivalent complex stiffness

In the mono axial case, the constitutive relation between the resulting compression force $\underline{F}$ and the displacement of the movable rigid surface $\underline{u}$ for a damping material subject to steady state harmonic excitations can be written as:

$$\underline{F} = \bar{K} \cdot \underline{u} \quad \text{with} \quad \bar{K} = K(1 + i\eta) \tag{13}$$

Where $\bar{K}$ is the equivalent complex stiffness, K the storage stiffness and η the loss factor. Typically, the loss factor is an image of the damping effect of such a device.

By considering the Valanis endochronic theory [11] and the approximation of the harmonic balance, it is possible to define the storage stiffness and the loss factor. After calculations, their expressions are respectively:

$$K\sqrt{1+\eta^2} = \frac{\omega}{\pi \cdot u_m}\sqrt{\left(\int_0^T f(t)\cos(\omega t)\,dt\right)^2 + \left(\int_0^T f(t)\sin(\omega t)\,dt\right)^2}, \tag{14}$$

$$\eta = \frac{\int_0^T F(t)\cos(\omega t)\,dt}{\int_0^T F(t)\sin(\omega t)\,dt} \tag{15}$$

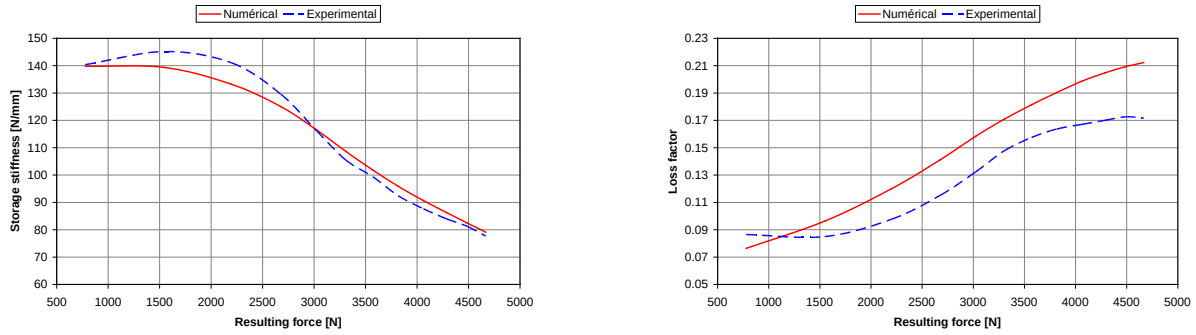

(a) (b)

FIG. 6 – Equivalent complex stiffness : storage stiffness (a) and loss factor (b) versus the resulting force.

Computed for each cycles (numerical and experimental ones) with a Matlab© subroutine, the figure 6 shows the evolution of the storage stiffness (a) and the loss factor (b) versus the compression force. An increase of

the loss factor (thus the damping effect) and a decrease of the storage stiffness is noticed with the resulting compression force.

4.2 Dynamic behavior

With this definition of the equivalent complex stiffness, the vibration equation (eq. 16) is solved, with $m = 1$ kg. The Bode diagrams are given on the figure 7. A typical non linear dynamical behavior is noticed.

$$m \cdot \ddot{u}(t) + k\left(1 + i\eta\right) \cdot u(t) = F(t) \tag{16}$$

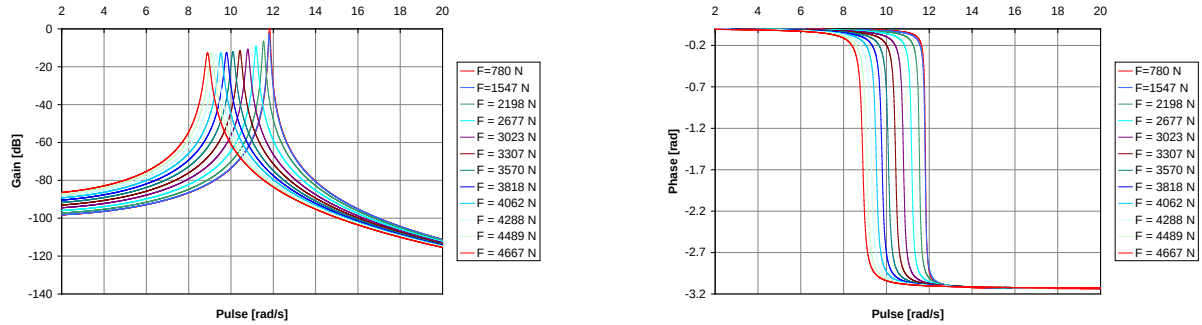

(a) (b)

FIG. 6 – Bode diagrams : gain (a) and phase (b)

5 Conclusion

In this communication, experimental and numerical compression tests on a SMA helical spring are presented. These investigations lead to investigate the damping effect with the innovative equivalent complex stiffness tool. Consequently, the dynamical behavior of such a device is performed and the non linear dynamical behavior of the spring is noticed. This new numerical modeling tool allows us to improve the non linear modeling of SMA devices in order to develop and optimize applications for control in civil engineering.

References

[1] Gandhi F., Wolons D.. Characterisation of the pseudoelastic damping behaviour of shape memory alloy wires using complex modulus. Smart Mat. & Struct., 8, 49-56, 1999.

[2] Bono F., Tirelli D., Characterisation of materials for the innovative antiseismic techniques, JRC ISPRA, Internal report, 1999.

[3] Tirelli D., Renda V., Bono F., Characterisation of shape memory alloys applications to the retrofitting of brick masonry wall by the pseudo-dynamic method and numerical models, JRC ISPRA, Internal report, 2000.

[4] Collet M., Foltete E., Lexcellent C., Analysis of the behaviour of a shape memory alloy beam under dynamical loading, Eur. J. Mech. A, 20, 615-630, 2001.

[5] Piedboeuf M.C., Gauvin R., Thomas M., Damping behavior of shape memory alloys : strain amplitude, frequency and temperature effects, J. Sound and Vibration, 214(5),895-901, 1998

[6] Speicher M. Hodgson D., Desroches R., Leon R., SMA tension/compression device for seismic retrofit building, JMPEG, 18, 746-753, 2009.

[7] Mirzaeifar R., Desroches R., Yavari A. A combined analytical, numerical, and experimental study of SMA helical springs, IJSS, 48, 611-624, 2010.

[8]Peultier B., Ben Zineb T., Patoor E., Macroscopic constitutive law of shape memory alloy thermomechanical behaviour. Application to Structure computation (b) FEM, Mechanics of Materials, 38, 510-524, 2006.

[9] Chemisky Y. Modélisation du comportement macroscopique des alliages à mémoire de forme. Application au matériaux composites, Thèse de doctorat, Université Paul Verlaine, 2009.

[10] Duval A. Modélisation du comportement thermomécanique d'alliages à mémoire de forme. Application au dimensionnement de microsystèmes et extension en non local, Thèse de doctorat, Université Henri Poincaré, 2009.

[11] Valanis K.C., A theory of viscoplasticity without a yield surface. Arch. Mech., 23, 517-551, 1971.